https://doi.org/10.25686/7231.2020.6.58829

COMPREHENSIVE EVALUATION OF ECOLOGICAL ENVIRONMENT IN DAZHANGXI BASIN BASED ON MULTI-SOURCE REMOTE SENSING DATA

Junjun Fang[1], Jinming Sha[1,2], Xuerui Guo[3], Gaopeng Sun[4], Qixin Lin[1]
[1]College of Geographical Sciences, Fujian Normal University, China
[2]China-Europe Environment Center, Fujian Normal University, China
[3]Wageningen University & Research, Netherland
[4]College of geography and tourism, Shaanxi Normal University, China

Ecosystem assessment plays an important role in ensuring regional ecological security and promoting the coordinated development of social economy and ecological environment protection. Remote sensing technology can objectively and quantitatively evaluate the spatial-temporal change of ecological environmental quality. This paper uses multi-source data to comprehensively analyze land surface temperature, land use and land cover, net primary productivity (NPP) and remote sensing ecological index in 2013 and 2017. The comprehensive evaluation system of the ecological environment in Dazhangxi basin is established by qualitative analysis of the ecological environment from multi perspectives and multi spatial and temporal scales. The results showed that: 1) The urban construction land at the intersection of Dazhongxi River and Minjiang River have expanded rapidly from 2013 to 2017, and the thermal environment effect is enhanced, forming local heat island effect. 2) The vegetation coverage in the study area is high, reaching more than 60%. Compared with 2013, the types of forest land and agricultural land decreased significantly in 2017, while the construction land and unused land increased significantly. 3) NPP showed a downward trend, and the reduction area was mainly forest. 4) Compared with 2013, the higher ecological and lower ecological zone decreased, while the medium ecological zone increased in 2017, which means the better ecological environment has been damaged and the areas with serious ecological environment problems have been partially improved. 5) During 2013-2017, the ecological environment of the study area showed a trend of slight deterioration, but it was alleviated by human intervention.

Keywords: *ecological environment, comprehensive assessment, dynamic monitoring, remote sensing technology, Landsat, Dazhangxi basin.*

Introduction

With the rapid development of economy and society, the ecological environment is inevitably suffering huge damages, such as losses of natural resources, reduction in biodiversity, environmental pollution and global climate change (Almeida et al., 2017; Chai, Lha, 2018; Ostrom, 2009). In order to achieve the goal of sustainable development, ecological environment has attracted more and more attention (Jing et al., 2020; Liu et al., 2018). Monitoring and comprehensive assessment of ecological environment, proposing protection measures and enhancing ecosystem services have become a hotspots in the field of environmental research. However, it is difficult to comprehensively evaluate the ecological environment due to its complexity and inherent interdisciplinary characteristics (Miao et al., 2016; Vorobyev et al., 2015).

Most of the previous studies evaluated the ecological environment from one or just a few aspects, which limits the accuracy of the assessment. Wang et al (2019) and Zhang et al (2020) reported the relationship between ecological environment and land use simulation, without considering other factors. Zheng et al (2020) reported the impact of urbanization on ecological environment. Li et al (2020) and Wang et al (2019) discussed the relationship between economy development and ecological environment. However, the reasonable integration of the above evaluation indicators into a comprehensive evaluation model requires more in-depth research.

Modern remote sensing earth observation system is widely used recently for the environmental evaluation study (Kurbanov, 2016; Jing et al., 2020). It provides multi-source data for extracting and synthesizing ecological evaluation indicators. Besides, remote sensing technology has great potential in large-scale monitoring and quality assessment of ecological environment (Kurbanov et al, 2014; Zhang et al., 2017; Niu, Wang, 2017). In 2006, the State Environmental Protection Ad-

ministration (2006) regulated the ecological environmental status index (EI) based on biological abundance index, vegetation cover index, water network density index, land degradation index, and environmental quality index. All of these indices have been widely applied in many research works. However, many scholars have tried different adjustments to the indices and weights due to the heterogeneity of different research regions (Zhu et al., 2017; Meng, Zhao, 2009). Therefore, EI cannot be used universally in different research areas.

Remote sensing ecological index (RSEI) is a new type of remote sensing based index for comprehensively ecological evaluation, the evaluation factors include greenness, heat, dryness and humidity, which are mainly obtained from satellite images (Gupta et al., 2012). These four indicators can be easily obtained and integrated into RSEI, thus easier to monitor regional ecological environment variation (Xu, 2013).

In China, different indicators reflect the ecological and environmental problems in different regions. One reason for this is the complexity and particularity of natural environmental conditions, the other is the long history of human activities and their profound impact on the ecological environment (Chai, Lha, 2018; Chi et al., 2018). Dazhangxi is the largest tributary of the lower Minjiang River in central Fujian Province, China. It plays an important role in regulating climate and maintaining ecological balance of the area. In addition, there have been limited studies on multitemporal and comprehensive ecological environment evaluation of this basin. Combined with the Comprehensive Planning of Fujian Dzhangxi Basin Report (Fujian Water Resources and Hydropower Institute, 2014), this study could give more detailed evaluation of the ecological environment in Dazhangxi.

The main purpose of this study is to provide scientific basis for ecological environment protection, comprehensive management, and sustainable development of Dazhangxi. Therefore, the following processes will be conducted in this study.

(1) Calculate the land surface temperature (LST), land use and land cover (LULC), net primary productivity (NPP) and RSEI in 2013 and 2017, respectively. (2) Analyze the ecological environmental indicators and their relationship between the two periods of the study area comprehensively and quantitatively. (3) Explore the spatial difference of ecological environment quality and discuss the results.

Material and Methods

Study area

Dazhangxi (at 118°59′14″ to 119°16′29″N latitude and 25°49′06″ to 25°59′32″E longitude) is the largest tributary of Minjiang River downstream, which is located in the central part of Fujian Province, China (fig.1). The drainage area of Dazhangxi is 4,843 km^2. The total length of the river is 234 km, and the average river slope is 2.1%. Dazhangxi has been the main waterway connecting the three coastal counties with the surrounding areas. The basin is rich in water resources and has many water diversion projects. Since the founding of the People's Republic of China, a large number of reservoirs and power stations have been built. This provides important conditions for local economic and social development. Meanwhile, due to human activities and hydropower development, the environment has been greatly affected.

Therefore, it is very important to quantitatively retrieve and monitor the LULC, LST, NPP and RSEI by remote sensing technology, which is beneficial to the protection of natural environment, human economy and ecology. It is not only real-time, rapid and accurate, but also significantly cost-effective in terms of manpower field investigation.

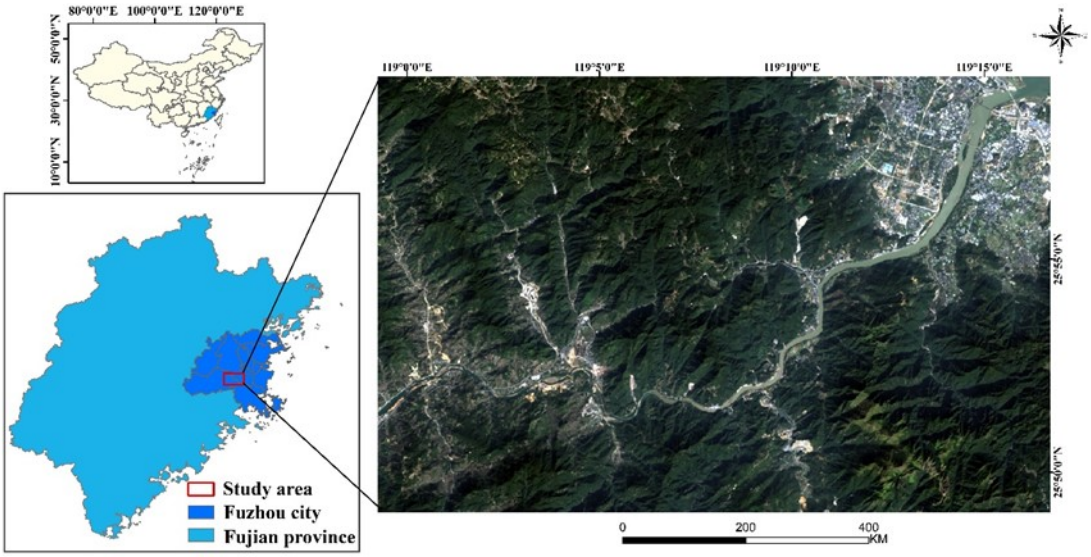

Fig.1. Location of study area and true color image

Methodology

The overall research process is shown in Fig. 2. It illustrates the framework for evaluating ecological environment using Landsat and ancillary data. The main steps include collection and preprocessing of remote sensing and other ancillary data, extraction of variables from remote sensing and ancillary data, evaluation of ecological environment from four aspects, and analysis of overall ecological environment of study area.

Data collection and preprocessing

Table 1 summarizes the data sets used in research, including two Landsat 8 images dated on October 23 of 2013 and December 21 of 2017, the ASTER Global Digital Elevation Model (GDEM), MODIS product data MOD11A1, weather station data, and the Comprehensive Planning of Fujian Dazhangxi Basin Report of this research area. Both Landsat images were calibrated by radiometric calibration, atmospheric correction and topographic correction in ENVI 5.5. GDEM with 30-m cell size were used for the topographic correction. Both images and GDEM data have the same Universal Transverse Mercator (UTM) coordinate system with World Geodetic. The pan sharpening method was used to fuse Landsat images to improve the spatial resolution for subse-

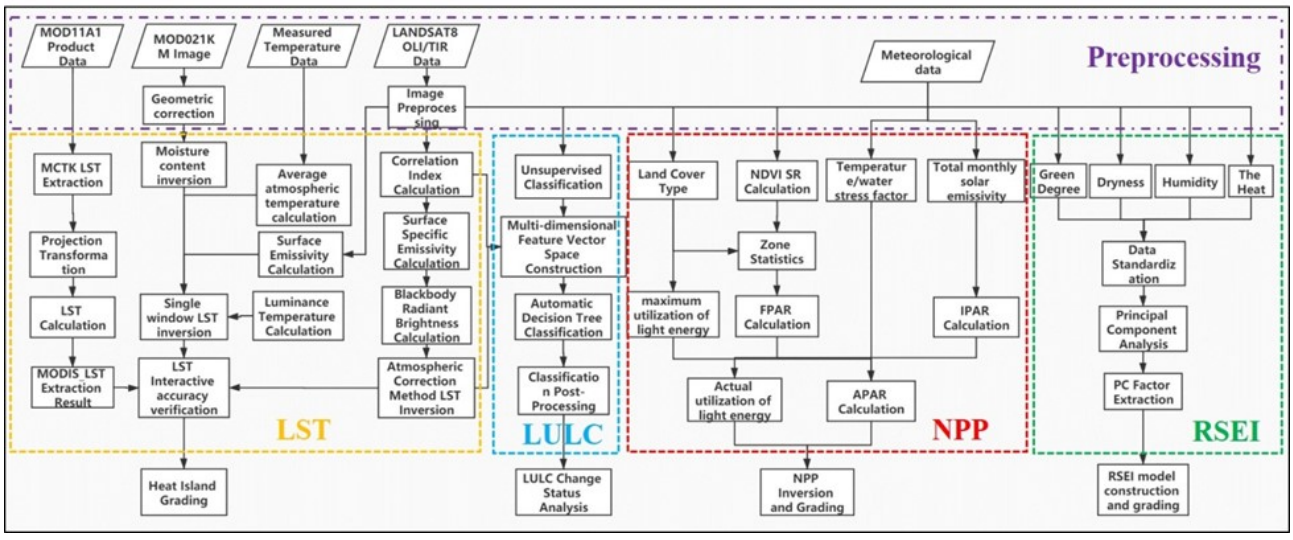

Fig. 2. The framework for ecological environment assessment

Table 1

Data sets used in research

Data sets	Description
Landsat 8 OLI images	Landsat 8 OLI images on October 23, 2013 (LC81190422013296LGN01) and December 21, 2017 (LC81190422017355LGN00)
30m GDEM	Aster Global Digital Elevation Model (GDEM)data with 30 m cell size
MOD11A1	Daily temperature product data
Weather station data	Daily rainfall and temperature data of Fujian in 2013 and 2017
Comprehensive Planning of Fujian Dazhangxi Basin Report	Environmental impact report on comprehensive planning of Dazhangxi Basin

Extraction of variables from remote sensing

Normalized difference vegetation index (NDVI), normalized difference building index (NDBI) and modified normalized difference water index (MNDWI) are used in this study. The principle of NDVI is that vegetation has different absorption in near-infrared band and red band. Vegetation information can be highlighted by calculation, so it is often used to characterize the coverage of surface vegetation. NDBI is a remote sensing index, which is used to distinguish urban and other building information. Xu (2005) proposed MNDWI on the basis of NDWI, which can better reveal the micro characteristics of water body. Their calculation is shown in Table 2.

Table 2

Calculation of indices

Indices	Calculation	Landsat 8 bands	Band math
NDVI	(ρNIR - ρR)/(ρNIR + ρR)	b5,b4	(b5-b4)/(b5+b4)
NDBI	(ρMIR - ρNIR)/(ρMIR + ρNIR)	b6, b5	(b5-b4)/(b5+b4)
MNDWI	(ρGreen - ρMIR)/(ρGreen + ρMIR)	b3,b6	(b3-b6)/(b3+b6)

Thermal environment model

(1) Impervious Surface Coverage (ISC)

The increase of ISC is a significant feature of urbanization and has a significant impact on regional ecological environment factors. In this study, normalized difference impervious surface index (NDISI) is used to extract impervious surface (Xu, 2008). Based on the spectral difference between impervious surface and other surface features, single band or multi band combination remote sensing is the most commonly used method to extract impervious surface. As a method that can automatically and quickly extract impervious surface in a large range, the principle of NDISI index is to construct strong reflection group and weak reflection group of impervious surface in spectral band of remote sensing image, and carry out band operation, so as to expand the contrast between impervious surface and sand soil, vegetation, water body and other surface features, so as to enhance the impervious surface information. The formula of the index is as follows:

$$NDISI = \frac{TIR - (MNDWI + NIR + MIR_1)/3}{TIR + (MNDWI + NIR + MIR_1)/3} \quad . \tag{1}$$

TIR, NIR and MIR_1 represent thermal infrared, near infrared and mid infrared bands of remote sensing image respectively, and MNDWI refers to modified normalized differential water index. Both MNDWI and TIR bands need linear stretching of 0-255 gray level to unify the quantization series of each band. The NDISI results were normalized and converted to ISC for further analysis.

The calculation formula is as follows:

$$ISC = \frac{NDISI_i - NDISI_{min}}{NDISI_{max} - NDISI_{min}} \times 100\% \ . \quad (2)$$

ISC is classified by mean-standard deviation method (table 3), which is also used in the following classification.

Table 3

Criteria for classification of impervious surface coverage

ISC levels	Division basis
First	$ISC_{mean+}s<ISC_{ni}$
Second	$ISC_{mean+}0.5s<ISC_{ni}\leq ISC_{mean+}s$
Third	$ISC_{mean}- 0.5s \leq ISC_{ni} <ISC_{mean+}0.5s$
Fourth	$ISC_{mean}- s \leq ISC_{ni}<ISC_{mean}- 0.5s$
Fifth	$ISC_{ni}<ISC_{mean} - s$

Note: ISC_{ni} is the normalized pixel value, ISC_{mean} is the average value of all pixels after normalization, *s is* the standard deviation.

(2) LST inversion

The atmospheric correction method and single window algorithm are used to retrieve the LST, and MOD11A1 are used to verify the accuracy. Finally, the LST retrieved by atmospheric correction method is selected to classify the heat island grade.

Atmospheric correction method: firstly, the influence of the atmosphere on the surface thermal radiation is estimated, and then this part of the atmospheric impact is subtracted from the total thermal radiation observed by satellite sensors to obtain the surface thermal radiation intensity, and then the thermal radiation intensity is converted into the corresponding surface temperature.

The brightness value L_λ of thermal infrared radiation received by the satellite sensor consists of three parts: the upward radiance of the atmosphere, the energy of the real radiance of the ground after passing through the atmosphere, and the reflected energy of the downward radiation from the atmosphere to the ground. The expression of thermal infrared radiance value L_λ received by satellite sensor (radiative transfer equation) can be written as:

$$L_\lambda = [\varepsilon_{B(T_s)} + (1-\varepsilon)L\downarrow]\tau + L\uparrow \ , \quad (3)$$

where, ε is the surface emissivity, T_S is the real surface temperature (K), $B(T_S)$ is the blackbody thermal radiance brightness, and τ is the atmospheric transmittance in the thermal infrared band. Then the radiance $B(T_S)$ of the blackbody with temperature T in the thermal infrared band is:

$$B(T_s) = [L_\lambda - L\uparrow - \tau(1-\varepsilon)L\downarrow] / \tau\varepsilon \ . \quad (4)$$

T_s can be obtained by the function of Planck's formula.

$$T_s = K_2 / \ln(K_1 / B(T_s) + 1) \ . \quad (5)$$

For TIRS band10, K_1 = 774.89 w / (M^2 * μm * sr), K_2 = 1321.08 K. LST is divided into five grades by means of mean-standard deviation method: high temperature zone, sub high temperature zone, medium temperature zone, sub low temperature zone and low temperature zone. Sub high temperature zone and high temperature zone are considered as heat island area.

(3) Vegetation fractional coverage (VFC)

The calculation of VFC was shown below:

$$FVC = (NDVI - NDVI_{soil}) / (NDVI_{veg} - NDVI_{soil}) . \quad (6)$$

According to the situation of remote sensing images, $NDVI_{soil}$ and $NDVI_{veg}$ are replaced by $NDVI_{min}$ and $NDVI_{max}$ respectively. Due to the inevitable noise, $NDVI_{min}$ and $NDVI_{max}$ generally take the maximum and minimum values within a certain confidence range, and the confidence values are mainly determined as 5% and 95% according to the actual situation of the image.

LULC classification

The automatic decision tree method is used to classify the images of Dazhangxi Basin in 2013 and 2017. The decision tree method obtains the classification rules through the experience of experts, simple mathematical statistics and induction methods, and carries out remote sensing classification. The classification rules are easy to understand, and the classification process is in line with human cognitive process, and the biggest feature is the use of multi-source data. NDVI, MNDWI, NDBI, ISC and LST are selected as auxiliary data for decision tree classification. According to the LULC classification standard in 1984, the land in the study area is divided into six categories: construction land, unused land, farmland, water body area, forest and grassland.

Two ROIs are drawn independently on Google Earth, which are used to model and verify the classification. According to the separability report of ROI, it is greater than 1.99, which proves that the selection of ROI is very reasonable. After classification, principal component analysis and cluster analysis are used to process the classification results.

NPP estimation

CASA model was used to retrieve NPP, considering the effects of solar radiation, temperature and precipitation. Based on Landsat 8 OLI and meteorological data, NPP estimation models for different land types in the Dazhangxi Basin were constructed. Compared with other NPP of vegetation at home and abroad, CASA model is more simple and convenient. The parameters can be determined respectively by using remote sensing information extraction and GIS, which avoids unnecessary errors caused by artificial simplification or estimation of parameters due to lack of parameters. The specific calculation process of CASA model is as follows:

$$NPP(x,t) = APAR(x,t) * \varepsilon(x,t) , \quad (7)$$

x is the spatial position and t is the time; NPP (x, t) is the NPP ($gC \cdot m^{-2} \cdot month^{-1}$) of pixel x in t month; APAR (x, t) is the photosynthetic effective radiation absorbed by pixel x in t month ($MJ \cdot m^{-2} \cdot month^{-1}$); Ɛ (x, t) is the actual light energy utilization rate of pixel x in month t ($gC \cdot MJ^{-1}$).

According to formula (7), NPP (x, t) is determined by APAR(x,t) and Ɛ(x,t), and APAR(x,t) can be calculated as (8):

$$APAR(x,t) = Q(x,t) * FPAR(x,t) * 0.5 , \quad (8)$$

Q (x, t) is the total solar radiation at pixel x in month t; FPAR (x, t) is the absorption ratio of incident photosynthetically active radiation by vegetation layer; the constant 0.5 represents the proportion of solar effective radiation (wavelength 0.38 ~ 0.71 μm) available for vegetation in total solar radiation. Ɛ(x,t) can be calculated as (9):

$$\varepsilon(x,t) = \varepsilon_{max} * T_{\varepsilon 1(x,t)} * T_{\varepsilon 2(x,t)} * W_{\varepsilon(x,t)} , \quad (9)$$

$T_{\varepsilon 1(x,t)}$ and $T_{\varepsilon 2(x,t)}$ denote the stress effect of low temperature and high temperature on light energy utilization efficiency, $W_{\varepsilon(x,t)}$ is the influence coefficient of water stress, and ε_{max} is the maximum

light energy utilization rate of vegetation under ideal conditions, which is related to vegetation types. The maximum photosynthetic utilization rate of Chinese typical vegetation simulated by Zhu et al (2006) was used here. In particular, the farmland in the study area are mainly evergreen broad-leaved forest and evergreen coniferous forest. According to the research results, the average value of evergreen broad-leaved forest and evergreen coniferous forest (0.687) is taken as the maximum light energy utilization rate of forest land.

(1) Calculation of Q(x,t)

$$Q(\mathrm{x},t) = Q_0 * （\mathrm{a+b}* \frac{n}{N}）, \tag{10}$$

Q is the monthly total solar radiation received by the earth's surface; Q_0 is the monthly astronomical total radiation; n/N is the percentage of monthly sunshine. a and b are empirical coefficients, which are taken as 0.25 and 0.50 respectively. FAO suggests that this should be set when no measured solar radiation data can be used and the accuracy correction of a and b parameters is not improved (Wang et al., 2014). The monthly total astronomical radiation Q_0 is calculated by the method of daily summation of the total astronomical radiation Q_i, and the daily total astronomical radiation is calculated by formula (11)

$$Q_{\mathrm{i}} = \frac{TG_{sc}}{\pi} * \rho^2 * (\omega_0 \sin\varphi \sin\delta + \cos\varphi \cos\delta \sin\omega), \tag{11}$$

Q_i is the total daily astronomical radiation ($MJ \cdot m^{-2} \cdot D^{-1}$); T is the period ($24 \times 60 \times 60s$); G_{SC} is the solar constant (13.67×10^{-4} $MJ \cdot m^{-2} \cdot s^{-1}$); ρ is the relative distance between the sun and the earth; ω_0 is the sunset angle (rad); φ is the geographical latitude (rad); δ is the solar declination (rad). The relative distance between the sun and the earth is calculated by equation (12).

$$\rho = \sqrt{\frac{1}{1 + 0.033\cos\frac{2\pi J}{365}}}, \tag{12}$$

J is the day ordinal number of a day in the year, from 1 January 1 to 365 December 31. The sunset angle ω_0 is calculated by equation (13)

$$\omega_0 = \arccos(-\tan\varphi \tan\delta). \tag{13}$$

The declination of the sun is calculated by equation (14)

$$\delta = 0.409\sin(\frac{2\pi J}{365} - 1.39). \tag{14}$$

(2) Calculation of FPAR (x,t)

Because the FPAR estimated by NDVI will be higher than the measured value, while the FPAR estimated by SR will be lower than the measured value, it is necessary to obtain the actual photosynthetic effective radiation absorption ratio (FPAR) by adjusting coefficient α (0.5 in this study).

$$FPAR(x,t) = \alpha * FPAR_{NDVI(x,t)} + (1-\alpha) * FPAR_{SR(x,t)}, \tag{15}$$

$FPAR_{NDVI(x,\,t)}$ and $FPAR_{SR(x,\,t)}$ are the proportion coefficients of photosynthetic effective radiation absorption of vegetation canopy calculated by NDVI and SR, respectively, which are calculated by (16) and (17).

$$FPAR_{NDVI(x,t)} = \frac{NDVI(x,t) - NDVI_{i,\min}}{NDVI_{i,\max} - NDVI_{i,\min}} * (FPAR_{\max} - FPAR_{\min}) + FPAR_{\min}. \tag{16}$$

In equation (16), NDVI(x, t) is the NDVI of pixel x in month t. $NDVI_{i,max}$ is the value of NDVI with confidence level of 95% for the i-th land cover type, and $NDVI_{i,min}$ is the value of NDVI confidence level of 5% for unused land; the values of $FPAR_{min}$ and $FPAR_{max}$ are 0.001 and 0.95, respectively.

$$FPAR_{SR(x,t)} = \frac{SR(x,t) - SR_{i,\min}}{SR_{i,\max} - SR_{i,\min}} * (FPAR_{\max} - FPAR_{\min}) + FPAR_{\min} , \quad (17)$$

SR(x, t) is the ratio vegetation index of pixel x in month t (18); $SR_{i,max}$ is the value of NDVI with confidence level of 95% for the i-th land cover type, and $SR_{i,min}$ is the value of NDVI confidence level of 5% for unused land; the values of $FPAR_{min}$ and $FPAR_{max}$ are 0.001 and 0.95, respectively.

$$SR(x,t) = \frac{1 + NDVI(x,t)}{1 - NDVI(x,t)} . \quad (18)$$

(3) Calculation of $T_{\varepsilon 1(x,t)}$

$$T_{\varepsilon 1(x,t)} = 0.8 + 0.02 * T_{opt}(x) - 0.0005 * [T_{opt}(x)]^2 , \quad (19)$$

$T_{opt}(x)$ is the optimum temperature for plant growth, which is defined as the average temperature of the month when the NDVI value reaches the highest in a certain region in a year. For the study area, the average temperature in July is taken as the optimum; when the average temperature in a certain month is less than or equal to -10℃, $T_{\varepsilon 1(x,t)}$ is taken as 0.

(4) Calculation of $T_{\varepsilon 2(x,t)}$

$$T_{\varepsilon 2(x,t)} = 1.184 / \{1 + \exp[0.2 * (T_{opt}(x) - 10 - T(x,t))]\} * 1 / \{1 + \exp[0.3 * (-T_{opt}(x) - 10 + T(x,t))]\} \quad (20)$$

When the average temperature of a month T(x, t) is 10℃ higher or lower than the optimum temperature $T_{opt}(x)$, the value of $T_{\varepsilon 2(x,t)}$ in the month is equal to half of the value of $T_{\varepsilon 2(x,t)}$ when the monthly average temperature T (x, t) is the optimal temperature $T_{opt}(x)$.

(5) Calculation of $W_{\varepsilon(x,t)}$

$$W_{\varepsilon}(x,t) = 0.5 + 0.5 * C(x,t) / C_p(x,t) , \quad (21)$$

C(x,t) is the actual regional transpiration (mm), which is calculated according to the regional actual evapotranspiration model established by Zhou and Zhang (1995) (Eq. 22); $C_p(x,t)$ is the regional potential evapotranspiration (mm), which is calculated according to the complementary relationship between EET and PET (Luo, 2010) (Eq. 23). The required parameter data are provided by monthly average temperature T(x, t) and monthly total precipitation W(x, t).

$$EET = \frac{r \bullet Rn(r^2 + Rn^2 + r \bullet Rn)}{(r + Rn) \bullet (r^2 + Rn^2)} , \quad (22)$$

$$2PET = Ep + EET , \quad (23)$$

r is the monthly accumulated precipitation (mm); R_n is the regional accumulated surface net radiation. Since many parameters for calculating the net surface radiation are difficult to obtain, they can be estimated by using the empirical model (Eq. (24)) established by Zhou and Zhang (1996).

$$Rn = (Ep \bullet r)^2 \times [0.369 + 0.598(\frac{Ep}{r})^{0.5}] , \quad (24)$$

Ep in equations (24) and (25) is local potential evapotranspiration (mm), which is calculated by using the vegetation climate relationship model (Thornthwaite, 1948) as formula (25).

$$Ep = 2037.98 - 18.8308LAT - 4.5801LONG - 0.157861ALT\ , \quad (25)$$

LAT is the latitude of the research site, LONG is the longitude of the research site, and ALT is the altitude of the research site.

NPP was divided into five grades by mean-standard deviation method: high biomass area, secondary high biomass area, medium biomass area, secondary low biomass area and low biomass area. The high biomass area and the secondary high biomass area were regarded as the areas with rich biomass.

RSEI ecological index

RSEI includes four important indicators of natural ecological environment: greenness, humidity, heat and dryness. Among the many natural factors reflecting ecological quality, these four factors are closely related to human survival, and are also the most important indicators for human beings to intuitively feel the quality of ecological conditions. Remote sensing technology can obtain the information of these four indicators from remote sensing images, such as vegetation index, humidity component, surface temperature and soil index to represent greenness, humidity, heat and dryness respectively

$$RSEI = f(NDVI, WET, LST, NDSI)\ , \quad (26)$$

NDVI is vegetation index; Wet is humidity component; LST is surface temperature; NDSI is soil index. NDVI is undoubtedly the most widely used vegetation index, which is closely related to plant biomass, leaf area index and vegetation coverage. Therefore, NDVI is selected to represent the greenness index. The brightness, greenness and wetness obtained by tassel cap transformation have been widely used in ecological environment monitoring. The humidity component reflects the humidity of water, soil and vegetation, which is closely related to ecology. Therefore, the humidity index of this study is represented by wetness:

$$WET = 0.0315\rho_1 + 0.2021\rho_2 + 0.3102\rho_3 + 0.1594\rho_4 - 0.6806\rho_5 - 0.6109\rho_7\ , \quad (27)$$

where: ρ_i(i = 1,...,5, 7) is the reflectivity of each band. LST uses the best atmospheric correction inversion results after the interactive accuracy verification of MOD11A1 data to obtain the index. The NDSI is selected as the dryness index. However, in the regional environment, there isa considerable number of construction lands, which also cause the drying of the surface. Therefore, the dryness index can be synthesized by the soil index (SI) and the building index (NDBI).

$$NDSI = (SI + IBI)/2\ , \quad (28)$$

where

$$SI = [(\rho_5 + \rho_3) - (\rho_4 + \rho_1)]/[(\rho_5 + \rho_3) + (\rho_4 + \rho_1)]\ , \quad (29)$$

$$NDBI = (\rho_5 - \rho_4)/(\rho_5 + \rho_4)\ , \quad (30)$$

Principal component analysis (PCA) is a multi-dimensional data compression technology which selects a few important variables by orthogonal linear transformation. In this study, PCA is used to integrate indicators. Before this transformation, we must normalize these indices and map their values to [0,1]. Finally, the RSEI based on PC1 is between [0,1]. The closer to 1, the better the ecology. The comprehensive representativeness of RSEI can also be analyzed from the correlation between RSEI and each index. The stronger the correlation between RSEI and each index is, the more comprehensively it can represent each index.

RSEI is divided into five grades by means of a mean-standard deviation method: excellent ecological area, sub optimal ecological area, medium ecological area, sub poor ecological area and poor ecological area.

Results and discussion

Remote sensing indices

(1) NDVI

Figure 3 is the overall trend of NDVI distribution in 2013 and 2017, the high values are mainly concentrated in the upper, middle and lower right parts of the basin, and the low values are distributed in the west and northeast of the basin. According to the distribution of power stations reported in the Report, it can be seen that the low value of NDVI in the study area is mainly spread around the power station location. The low value in the northeast is mainly caused by the underlying surface being residential area. The NDVI value in 2017 was generally lower than that in 2013. It is obvious that taking the power station as the center, the relevant building land has been built or expanded around it, and the road facilities connecting the main stream of Dazhangxi and the power station have been built, which has affected the NDVI value of the whole research basin to a certain extent, and has an impact on the ecological environment.

(2) MNDWI

There is no significant difference in the distribution of MNDWI values between the two years (fig. 4). However, due to the fact that the image of 2013 is October and the image of 17 years is December, it is obvious that the discharge of 2017 is less than that of 2013 in the main part of Dazhangxi, especially in the west of the trunk part.

(3) NDBI

Compared with 2013, the building area increased in 2017 (fig. 5), and the fragmentation of building patches increased. In the western part of the basin, the increase is obvious in the western part of the basin, while the increase in other parts is not obvious, but the patch becomes more fragmented. This may be due to the construction of power stations in the basin and the intervention of human activities.

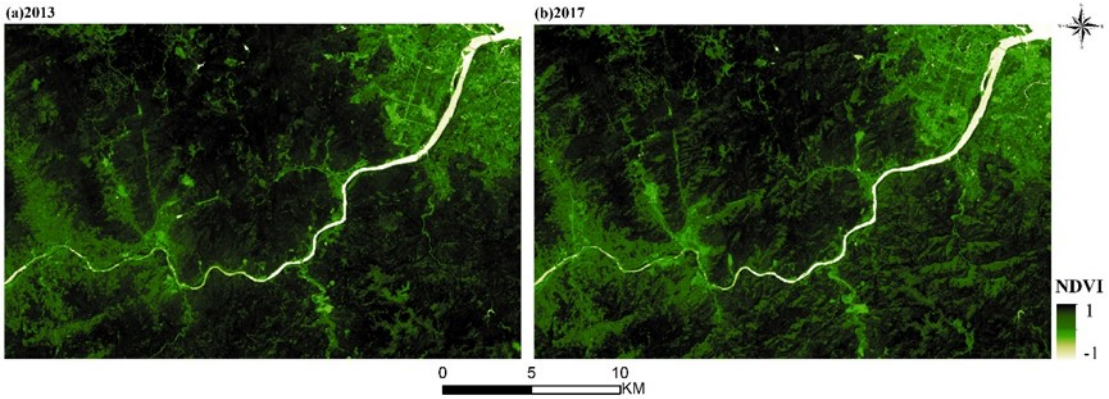

Fig. 3. NDVI of 2013 and 2017

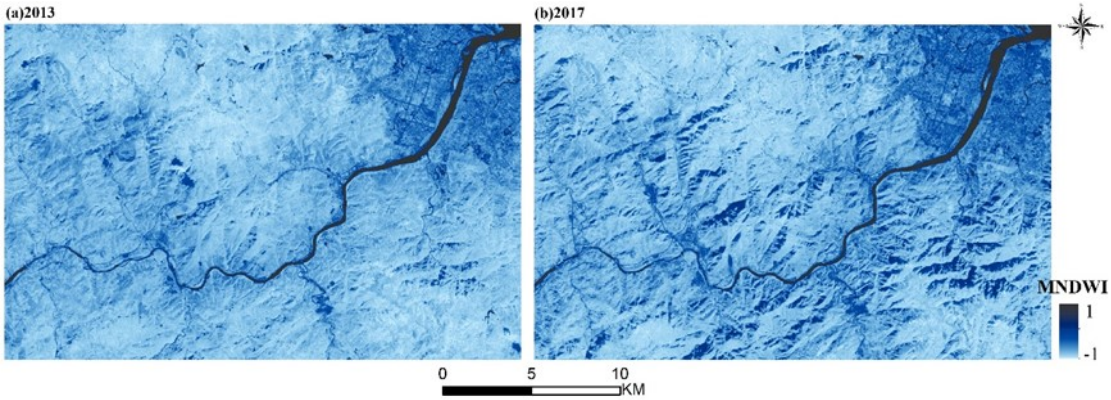

Fig. 4. MNDWI of 2013 and 2017

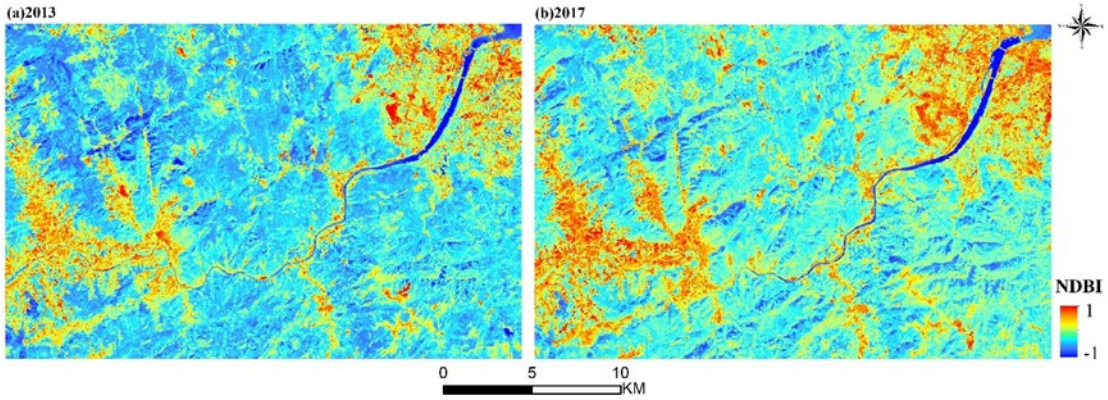

Fig. 5. NDBI of 2013 and 2017

Thermal environment

ISC

As can be seen from figure 6, compared with 2013, the first-class area in 2017 decreased, the second-class area increased slightly, the third-class area increased more significantly, and the area of fourth and fifth class areas decreased significantly. Combined with the situation of the study area, from 2013 to 2017, the buildings developed from contiguous to scattered, the road area increased, the forest area decreased, and the forest land gradually developed to sparse forest land.

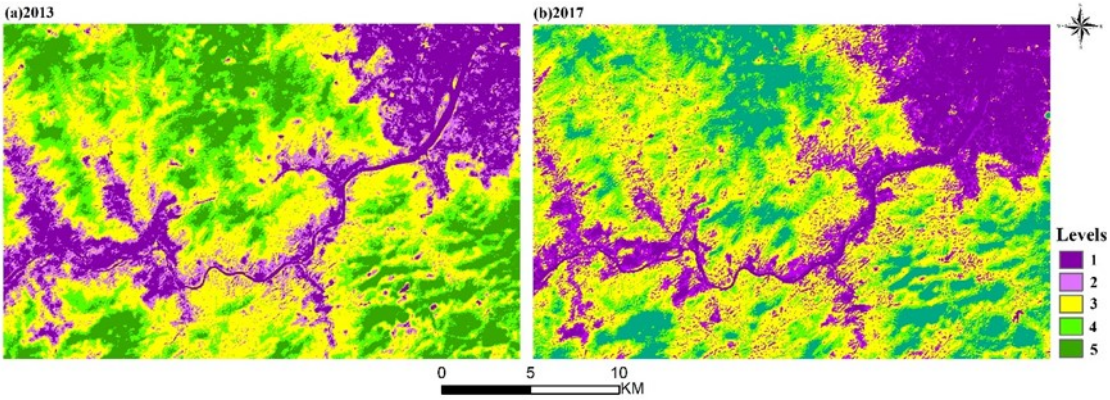

Fig. 6. ISC of 2013 and 2017

LST

Using the MOD11A1 data, the real LST of the study area was extracted. 200 random points are created in the research area. After resampling the atmospheric correction and single window algorithm inversion results, the temperature values of corresponding points are extracted. After the relevant data processing and regression model establishment, the correlation coefficient and R^2 were obtained. The specific results are shown in figure 7. In the two years, the atmospheric correction method is better in 2017, and the single window algorithm is better in 2013. However, the temperature of single window algorithm in 2017 is compressed in a narrow range, overall the atmospheric correction method is better. The following analysis is based on the results of atmospheric correction.

The LST results after grading are shown in figure 8. According to the final LST distribution map, combined with the ISC index classification results, the construction land in the downstream and along the banks of the Dazhangxi Basin has a significant heat island effect in 2013-2017. It can be concluded that LST and ISC results are significantly related to the degree of urbanization, but may also be restricted by vegetation, water and other factors. For example, the greening and environmental improvement in the central urban area may reduce its thermal environment effect to a certain extent.

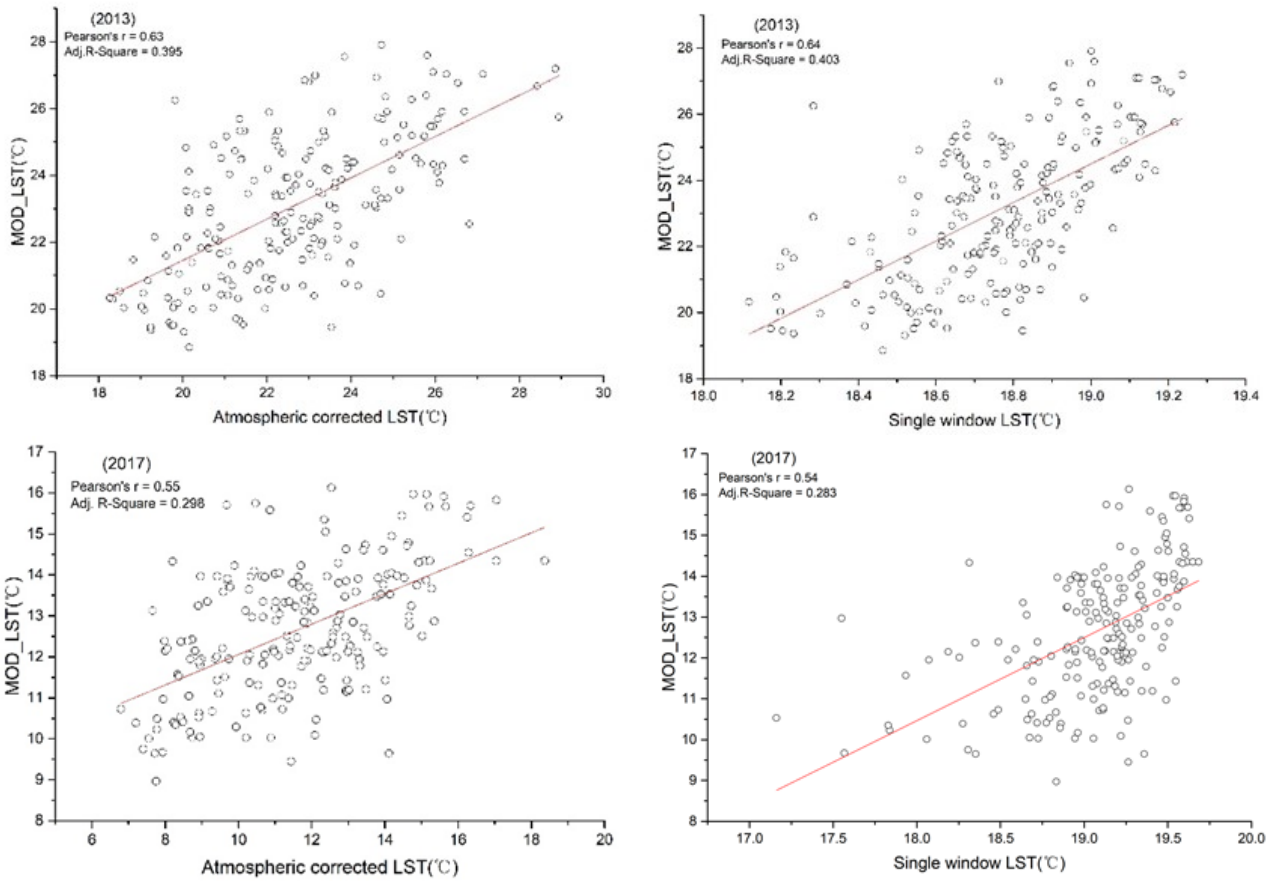

Fig. 7. LST regression model in 2013 and 2017

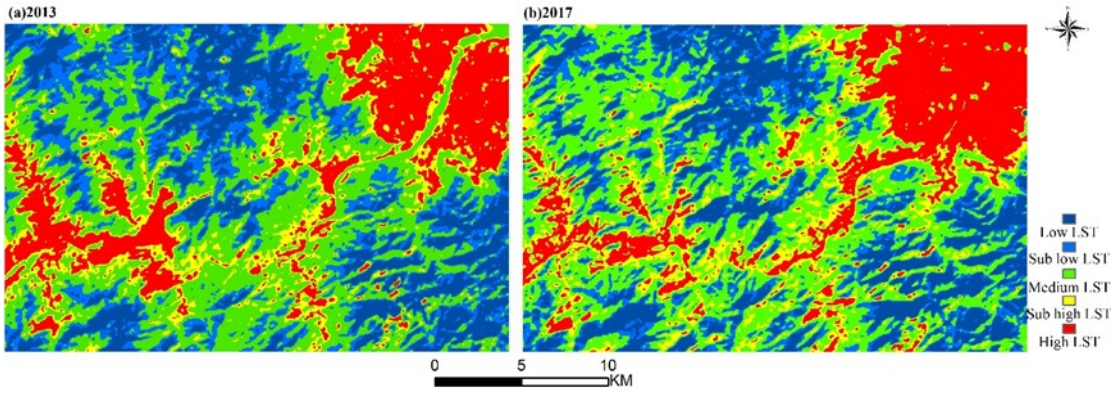

Fig. 8. LST levels distribution map in 2013 and 2017

VFC

Through comparative analysis, it can be found that the vegetation coverage in 2017 has an obvious trend of reduction, especially in the northeast and west of the basin, the vegetation area decreased significantly. In the southeast of the basin, there are also some areas where the vegetation coverage decreases. The main reason is that the operation of the power station needs some human intervention, which leads to the destruction of the ecological environment.

LULC monitoring and change detection

The classification accuracy based on the automatic decision tree method was 94.14% in 2013 and 90.69% in 2017, and the kappa coefficient was 0.92 and 0.88, respectively. The images of Dazhangxi watershed in 2013 and 2017 are classified, and the classification results are shown in figure 10.

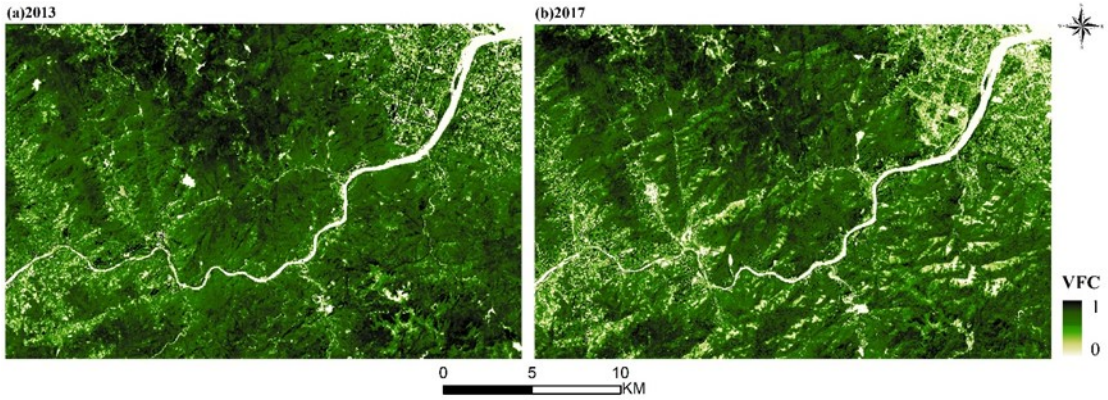

Fig. 9. VFC in 2013 and 2017

The construction land is mainly distributed along the river and mainly distributed in the northeast of Dazhangxi Basin, while the farmland is mainly distributed near the construction land. Compared with the land use map of 2013 and 2017, it can be found that the changes of construction land, farmland and unused land are more obvious. In 2017, the area of construction land increased, the area of agricultural land decreased, and the area of unused land increased.

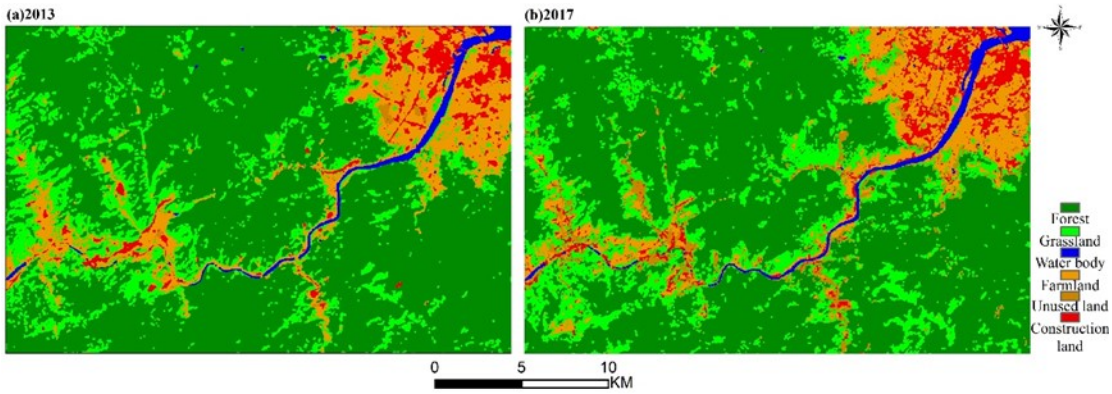

Fig. 10. LULC in 2013 and 2017

The classification results were statistically analyzed and a pie chart was drawn (fig. 11). The vegetation coverage rate of Dazhangxi basin is higher, reaching more than 60%. However, the vegetation coverage rate in 2017 was lower than that in 2013, the proportion of forest land and farmland decreased significantly, and the proportion of construction land and unused land increased significantly. This shows that with the advancement of urbanization, the land use in the Dazhangxi Basin has changed. The land use inclines to the construction land, and part of the farmland is used for urban construction. To a certain extent, this has affected the vegetation coverage rate and ecological environment of Dazhangxi Basin.

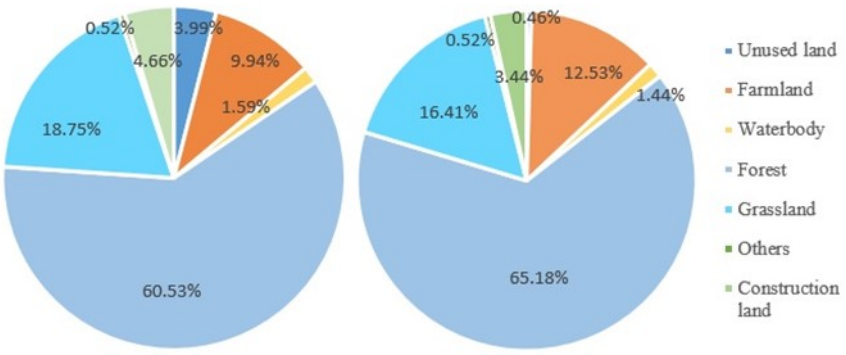

Fig. 11. Proportion of land use types in 2013 and 2017

In order to further reflect the land use change of Dazhangxi River Basin from 2013 to 2017, the concept of land transfer matrix (Liu, Zhu, 2010) was introduced and calculated the detailed land use type area transfer change from 2013 to 2017, as shown in table 4.

From the perspective of land transfer, the land with large transfer-out area was forest land, grassland and farmland in order from 2013 to 2017, with the transfer-in area of 33952.59 ha, 210725.66 ha and 7175.61 ha respectively. The largest transfer-in area was forest land, grassland and farmland, and the transfer area was 30559.86 ha, 11795.31 ha and 5665.23 ha respectively. The overall situation of the transfer in and out shows a decreasing trend in forest land, and it is mainly converted into grassland, and the construction land shows an increasing trend, and the main source of increase is the conversion of farmland to construction land.

From the area ranking, the vast majority of land types in Dazhangxi basin are forest land, grassland and farmland. Forest land is an important indicator of the natural and ecological environment in the region, which indicates that the ecological maintenance of Dazhangxi basin is relatively good. However, compared with 2013, the proportion of forest land decreased in 2017, and it was mainly transferred out to grassland, and the forest land and grassland were transformed from each other, mainly due to the impact of human activities. The proportion of construction land is increased, and it mainly comes from the conversion of farmland. Urban construction needs new expansion. But maintaining enough farmland area is also the key to ensure the economic and food sources of urban residents. While promoting the construction of urbanization, the Dazhangxi river basin should take into account the protection of ecological environment, so as to realize sustainable development.

Table 4

Land use change area transfer matrix from 2013 to 2017 (ha)

Land use	Grassland	Construction land	Forest	Farmland	Water body	Unused land	Transfer-out
Grassland	4984.29	219.87	3612.24	1147.32	5.4	756.54	10725.66
Construction land	29.25	904.68	5.22	675.18	71.55	263.43	1949.31
Forest	5778.63	39.87	26871.39	287.01	4.59	971.1	33952.59
Farmland	994.32	1310.58	70.65	3424.68	37.98	1337.4	7175.61
Water body	2.43	17.73	0.09	28.44	745.2	18.99	812.88
Unused land	6.39	155.43	0.27	102.6	12.6	131.58	408.87
Transfer-in	11795.31	2648.16	30559.86	5665.23	877.32	3479.04	55024.92

NPP monitoring and analysis

The NPP grading distribution in 2013 and 2017 was finally as shown in figure 12. Through comparative analysis, we can see that compared with 2013, the low biomass areas in 2017 increased significantly. Taking the main trunk of Dazhangxi as the center, the areas around it are almost all low biomass areas, and they are shown in a more contiguous form. However, the NPP inversion results in 2013 showed that there were a few high or sub high biomass areas in the form of broken patches near the main trunk of Dazhangxi. The main reason for this phenomenon is that the operation of the power station near the basin has destroyed the forest around it, thus affecting the biomass of the area. Another obvious change is that the high biomass area in 2017 has a certain reduction compared with 2013. Especially in the west, North and southeast of the basin, this situation is obvious.

The results of the changes of two years are detected as figure 13. On the whole, the NPP of the study area showed a decreasing phenomenon, and the decreasing area was mainly forest land type, which indicated that the forest land was affected in this process. There is a high spatial correlation between the unchangeable region and the low biomass area. The low biomass area is mainly water

land type. The biomass of water body is generally very low. It is impossible to develop into forest land type with high NPP in a short time. The NPP corresponding to all water body types will remain unchanged. The rising areas are mainly distributed in forest, especially in the East and West of the basin. In order to improve the ecological living conditions of local residents, some green belts were planted by human intervention. The NPP in Western China will increase sporadically, which is mainly due to the comprehensive utilization of Longxiang reservoir from power generation to water supply. This location has a certain ecological mitigation effect on this area.

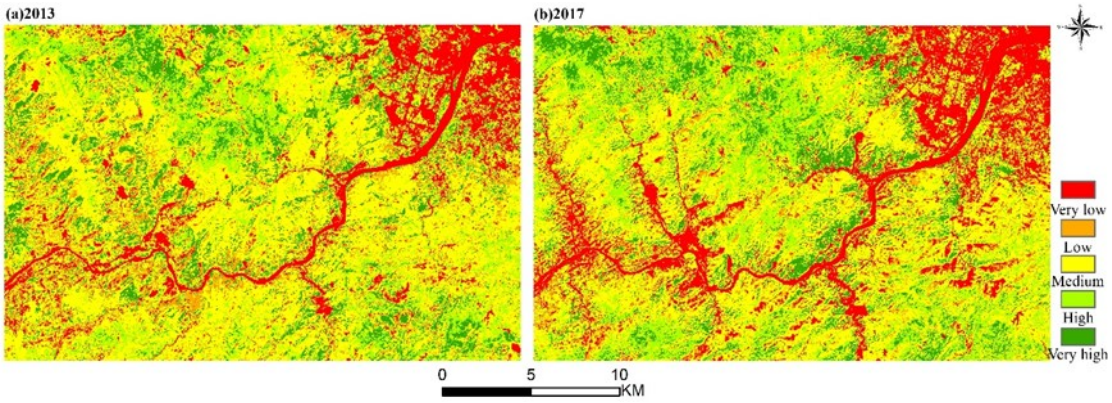

Fig. 12. NPP distribution map in 2013 and 2017

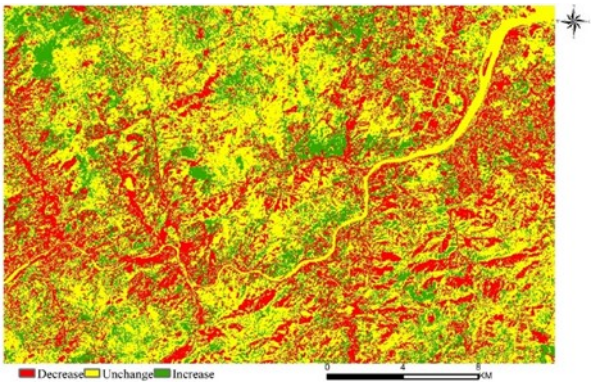

Fig. 13. NPP transform detection distribution

The NPP results, LST and VFC values of two periods was extracted by creating 200 random points in the study area. Statistical software was used to describe the spatial relationship among them. The results are shown in the figure 14.

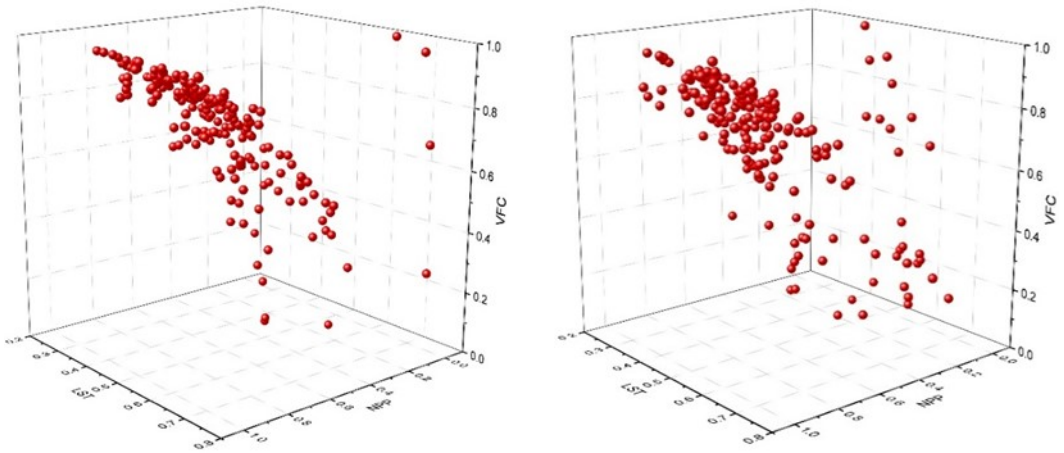

Fig. 14. Scatter map of 3D feature space (left 2013, right 2017)

According to the above analysis, NPP has a high correlation with VFC. With the increase of VFC, NPP increased except for a few sites. VFC, to a certain extent, represents the dense situation of ground vegetation. When the vegetation is lush, it can make full use of solar radiation and produce more NPP. Analysis of a small number of special points shows that NPP is always low no matter how the VFC changes, which may be caused by the model method. The calculation of the absorption of incident photosynthetically active radiation (PAR) by vegetation layer is based on different types of surface features. This study cannot guarantee that each type of ground feature can be identified completely and correctly. The corresponding pixel of this point may have vegetation surface feature spectral information and has high VFC, but its corresponding NPP value is underestimated because the ground feature type is not classified into vegetation.

In addition, there is no direct correlation between NPP and LST. In different temperature ranges, the corresponding NPP values are basically the same. In this study, we use the remote sensing image obtained at a certain time, and the temperature retrieved from it is also instantaneous, which will not have a direct impact on NPP. On the other hand, the study area is the Dazhangxi basin with a small scope. Even though different types of surface features have an impact on surface temperature, the overall impact is small, so the impact of temperature on net primary productivity is not obvious in this region.

RSEI monitoring and assessment

As can be seen from the table 5, The first principal component (PC1) of the four indicators in the study area has the following characteristics: 1) The contribution rate of PC1 is greater than 70%, indicating that it has concentrated most of the characteristics of the four indicators; 2) The four indicators have a certain degree of contribution to PC1, and are relatively stable, not like in other characteristic components (PC2 ~ PC4). 3) In PC1, NDVI and WET which represent the greenness and humidity are positive, indicating that they contribute positively to the ecology. LST and NDSI, which represent heat and dryness, are negative in PC1, indicating that they have negative effects on ecology, which is consistent with the actual situation. However, in PC2 ~ PC4, these indicators are sometimes positive and sometimes negative, which is difficult to explain the ecological phenomenon. Therefore, compared with other components, PC1 concentrates the characteristics of each index to the greatest extent, and can reasonably explain the ecological phenomenon, so it can be used to create comprehensive ecological index.

Table 5

Results of principal component analysis

Indices	2013				2017			
	PC1	PC2	PC3	PC4	PC1	PC2	PC3	PC4
dryness	-0.955	0.023	-0.249	0.157	-0.903	0.222	-0.327	0.169
greenness	0.841	0.526	0.084	0.096	0.713	0.654	0.239	0.085
heat	-0.891	0.024	0.452	0.040	-0.816	-0.171	0.547	0.071
humidity	0.875	-0.456	0.108	0.120	0.867	-0.468	-0.021	0.173

According to PC1, the comprehensive representativeness of RSEI can also be analyzed from its correlation with each index. The stronger the correlation between RSEI and each index is , the more comprehensively it can represent each index. Table 6 shows the correlation coefficient between each index and RSEI, as well as the correlation coefficient between each index itself. For a single indicator, the highest average correlation between indices is NDSI, reaching 0.849 in 2013, The two-year average is 0.792. However, the annual average correlation coefficient between RSEI and these four indicators is greater than 0.61, and the two-year average is 0.725, which is 6.4% higher than the average of the lowest NDVI. Obviously, the higher correlation between RSEI and

each index indicates that it is more representative than any single index and can comprehensively represent the information of each index.

Table 6

Correlation coefficient matrix of each index and RSEI index

Indices	2017					2013				
	NDSI	NDVI	LST	WET	RSEI	NDSI	NDVI	LST	WET	RSEI
NDSI	1	-0.562	0.532	-0.85	-0.678	1	-0.797	0.745	-0.855	-0.692
NDVI	-0.562	1	-0.557	0.322	0.819	-0.797	1	-0.694	0.516	0.812
LST	0.532	-0.557	1	-0.627	-0.701	0.745	-0.694	1	-0.737	-0.667
WET	-0.85	0.322	-0.627	1	0.729	-0.855	0.516	-0.737	1	0.698
Average correlation	0.736	0.610	0.679	0.700	0.732	0.849	0.752	0.794	0.777	0.717
Two year average	NDSI=0.792 NDVI=0.681 LST=0.737 WET=0.738 RSEI=0.725									

Note: the average correlation is calculated based on the absolute value of the correlation coefficient between itself and other indicators. Take NDSI in 2017 as an example: average correlation NDSI = [|-0.562| + |0.532|+|-0.85|+|1|]/4=0.736.

RSEI can also be used to establish ecological models to simulate and predict the trend of regional ecological change. Firstly, the thematic images of NDVI, WET, LST, NDSI and RSEI of each year are sampled, and then the relationship model is established by stepwise regression analysis with RSEI as dependent variable and NDVI, WET, LST and NDSI as independent variables, 28000 sample points were collected from each image. Enough sample points and sampling method throughout the whole image can ensure the representativeness and objectivity of regression analysis results, and avoid the uncertainty caused by small sample and local sampling. In 2013, the model is RSEI = 0.277Wet + 0.266NDVI– 0.302NDSI – 0.282LST+ 0.477 (R^2 = 0.992); while in 2017, it is RSEI = 0.313Wet + 0.258NDVI– 0.326NDSI – 0.295LST+ 0.483 (R^2 = 0.989). From the regression coefficient of each index, the coefficients of NDVI and WET are positive, indicating that they have positive effect on RSEI, while LST and NDSI are negative. Further study on the change of regression coefficient shows that the comprehensive influence of NDVI and WET on RSEI is more than that of NDSI and LST, because the sum of the two coefficients is greater than the absolute sum of NDSI and LST.

The RSEI grading results was shown in the figure 15. Compared with 2013, the low biomass areas in 2017 increased significantly. Taking the main trunk of Dazhangxi as the center, the areas around it are almost all low biomass areas, and they are shown in a more contiguous form. However, the NPP inversion results in 2013 showed that there were a few high or sub high biomass areas in the form of broken patches near the main trunk of Dazhangxi. The main reason for this phenomenon is that the operation of the power station near the basin has destroyed the forest around it, thus affecting the biomass of the area. Another obvious change is that the high biomass area in 2017 has a certain reduction compared with 2013. Especially in the west, North and southeast of the basin, this situation is obvious.

Figure 16 shows the results of changes between the two periods. Overall, the NPP of the study area showed a decrease, and the decrease area was mainly forest land type, which indicated that forest land was affected in this process. There is a high spatial correlation between the unchangeable region and the low biomass area. The low biomass area is mainly water body. The biomass of water body is generally very low. It is impossible to develop into forest with high NPP in a short time. The NPP corresponding to all water body types will remain unchanged. The rising areas are mainly distributed in forest, especially in the East and West of the basin. In order to improve the ecological living conditions of local residents, some green belts were planted by human intervention. The NPP in Western also increased sporadically, which is mainly due to the comprehensive

utilization of Longxiang reservoir from power generation to water supply. The development orientation has a certain ecological mitigation effect on the region.

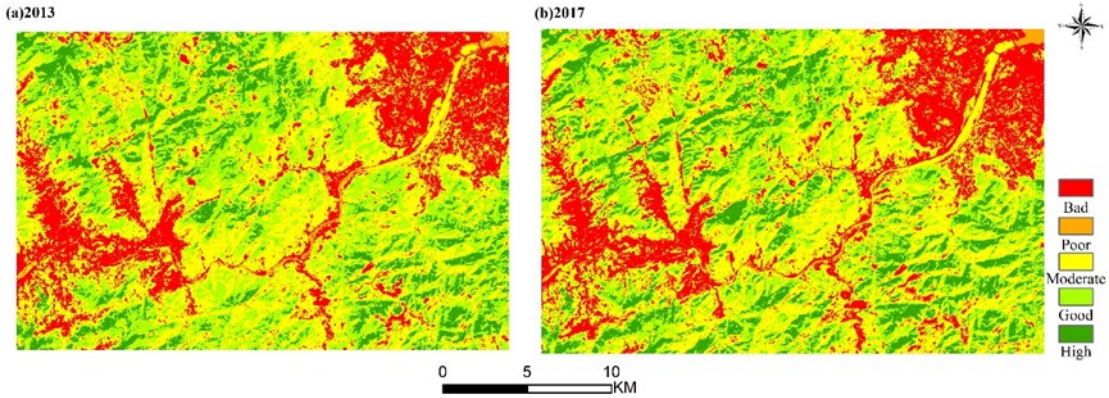

Fig. 15. RSEI grade distribution map

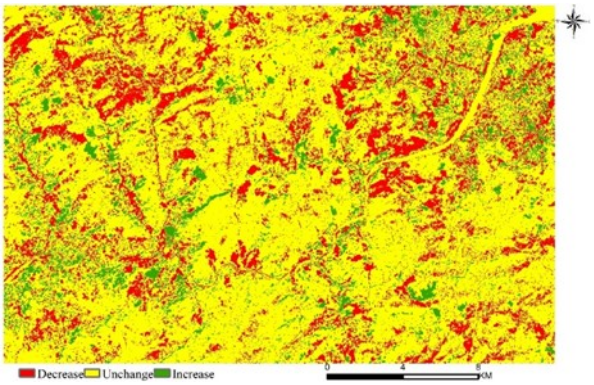

Fig. 16. RSEI transform detection distribution

The relationship between each index and the RSEI is investigated from the distribution of their scatter points in the 3-D characteristic space (fig. 17). The top of the scattered point group is the gathering area with good ecological conditions, mainly the high coverage vegetation area; the bottom end of the scattered point group is the gathering area with poor ecological conditions, representing the bare soil area. Generally speaking, both regression model and PCA show that the greenness represented by NDVI and the dryness represented by NDSI have the greatest impact on the ecological environment, and the impact of NDVI is greater than that of NDSI. The results of this data simulation also prove that the effect of controlling soil and water loss by increasing greenness in this area is greater. If the 2017 model is used for prediction, the NDVI will be increased by 0.253 for every 0.1 increase of RSEI.

Comprehensive evaluation of ecological environment

From the perspective of thermal environment, due to the rapid expansion of urban construction land along the banks of Dazhangxi, the intersection of tributaries and Minjiang River downstream, the thermal environment effect has been increasing, forming the local heat island effect. This has quite negative effect on ecological environment

As for land use change, the vegetation coverage rate of the study area is higher as a whole, reaching more than 60%. In 2017, compared with 2013, forest land and farmland declined obviously, while construction land and unused land have a large increase. This shows that with the advancement of urbanization, the land use in the Dazhangxi River Basin has changed significantly. The land use inclines to the construction land, and some forest land and farmland have changed into urban construction land. This phenomenon also damaged ecological environment to some extent.

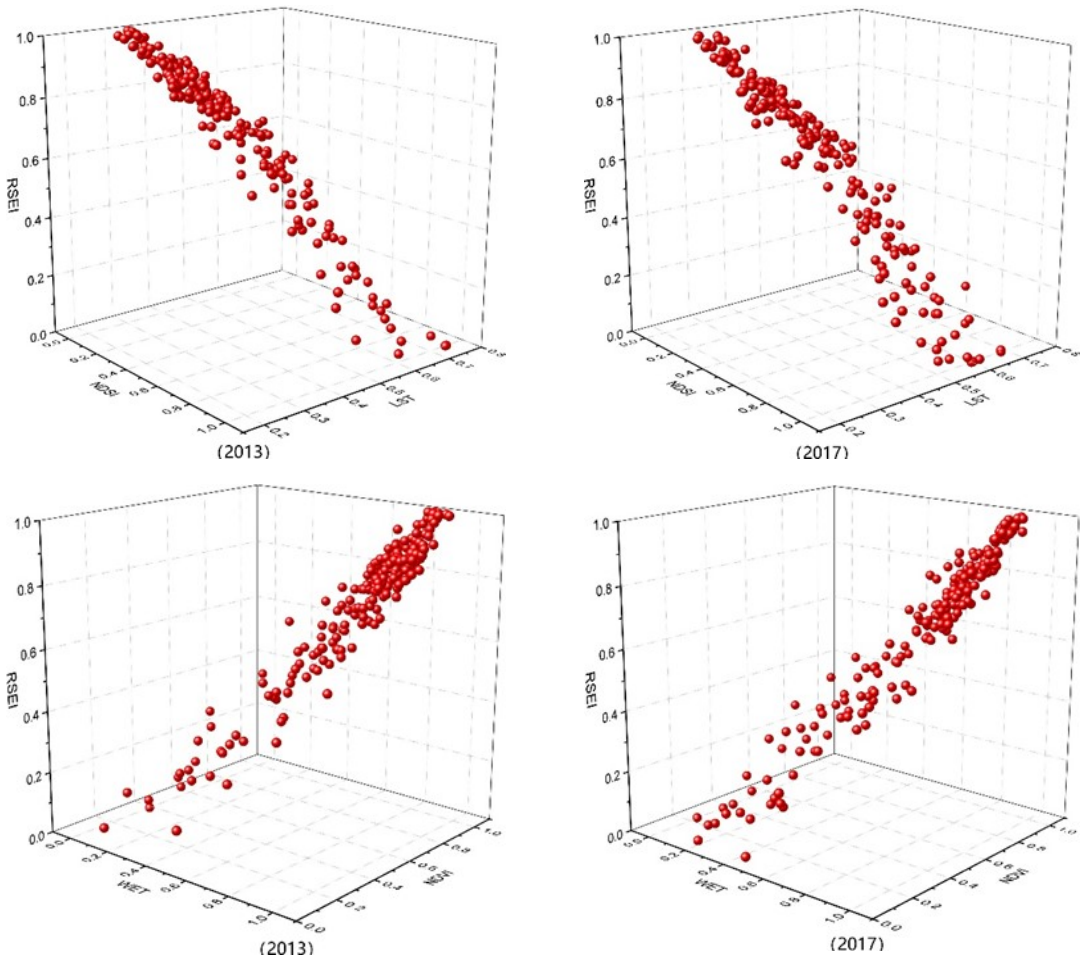

Fig. 17. Relationship between RSEI and variables

The NPP of the study area decreased in 2017, and the decreasing area was mainly forest land type. There is a high spatial correlation between the unchangeable area and the low biomass area, which is mainly caused by the water body in the low biomass area. The increasing areas are scattered in forest, especially in the East and West of the basin. This is mainly caused by the improvement of human intervention and the comprehensive utilization of Longxiang reservoir from power generation to water supply, taking into account power generation and other comprehensive utilization.

From the analysis of RSEI, compared with 2013, the area of excellent ecological area decreased significantly, the area of medium ecological area increased, and the area of poor ecological area decreased. This shows that in the process of these years, the areas with good ecological environment have been damaged to a certain extent, and the areas with serious ecological environment have been improved to a certain extent, making the ecological situation in 2017 mostly in the middle level.

Combined with the above analysis, from 2013 to 2017, the ecological environment of Dazhangxi Basin showed a slight deterioration trend, but due to human intervention, it has been improved to a certain extent in the later stage. Ecological environment plays an important role in people's quality of life. While planning urban construction, the local government should pay attention to the local conditions. At the same time, it should pay attention to the problems of urban expansion and forest land protection, avoid excessive concentration of heat island effect, so as to ensure the normal and balanced development of the region. In addition, the Dazhangxi basin is responsible for water supply, power generation, shipping and other important social functions in Fuzhou. Therefore, it is necessary to focus on measures such as increasing awareness of environmental protec-

tion, paying attention to ecological balance and reducing pollution emissions for urban construction land along the Bank of Dazhangxi. For the unreasonable and inefficient power station, we should make a comprehensive plan and change its main functions, so as to improve the ecological environment of the region and inject inexhaustible power into the sustainable development of the ecological environment in this area.

Conclusion and Recommendation

Through the combination of multi-source remote sensing data and a large number of field measured data, this work comprehensively evaluates the ecological environment of the study area from four aspects: thermal environment, LULC, NPP and RSEI, which provides certain reference and auxiliary decision-making basis for relevant government departments in planning and governance.

From four aspects, the ecological environment of Dazhangxi River Basin has been damaged in 2013-2017, but it has been improved in the later stage due to human intervention. Therefore, compared with 2013, the excellent ecological area and poor ecological area in 2017 have decreased, while the ecological area in the middle level has increased to a certain extent. In the reduced area, the land use mainly comes from forest land, and the ecological environment around the power station has been compensated and improved According to the current ecological environment of the study area, the following suggestions are put forward: 1) When planning urban construction, the government should pay attention to local conditions and speed up appropriately, avoid excessive concentration of heat island effect, and ensure the balance of regional development trend. 2) The unreasonable and inefficient power stations in the basin should be comprehensively planned to change their main functions and improve the ecological environment.

Although this paper quantitatively evaluated the ecological environment of the study area from many aspects, there are still many factors that affect the ecological environment do not consider, such as soil terrain factors, biological resources, etc. (Chang et al., 2019). The evaluation of this study is to evaluate the ecological environment from every single aspect, but not form a comprehensive index. The future research can combine the local characteristics, comprehensively consider the factors affecting the ecological environment, and create an integrated framework, so as to make a more comprehensive and accurate evaluation of the study area. Because of its special function orientation of power supply and transportation, the ecological environment of Dazhangxi basin is inevitably disturbed by human beings. In the future, human factors can also be quantified as an indicator to evaluate the ecological environment more accurately.

The paper was supported by EU Erasmus+ project "GIS and Remote Sensing for Sustainable Forestry and Ecology (SUFOGIS)" (598838-EPP-1-2018-EL-EPPKA2-CBHE-JP), "Innovation on Remote Sensing Education and Learning (IRSEL)"(586037-EPP-1-2017-1-HU-EPPKA2-CBHE-JP", and Chinese MOST international cooperation program "Using geospatial technology to monitor and assess the impact of land use / land cover change on Regional Ecological Security"(2018YFE0184300).

The European Commission support for the production of this publication does not constitute an endorsement of the contents which reflects the views only of the authors, and the Commission cannot be held responsible for any use which may be made of the information contained therein.

References

1. Almeida T.A. das N., Cruz L., Barata E., García-Sánchez I. M. Economic growth and environmental impacts: An analysis based on a composite index of environmental damage. *Ecological Indicators*, **2017**, *76*, 119-130. https://doi.org/10.1016/j.ecolind.2016.12.028 .
2. Chai L.H., Lha D. A new approach of deriving indicators and comprehensive measure for ecological environmental quality assessment. *Ecological Indicators*, **2018**, *85*, 716-728. https://doi.org/10.1016/j.ecolind.2017.11.039 .

3. Chang Y., Hou K., Wu Y., Li X., Zhang J. A conceptual framework for establishing the index system of ecological environment evaluation – A case study of the upper Hanjiang River, China. *Ecological Indicators*, **2019**, *107*. https://doi.org/10.1016/j.ecolind.2019.105568
4. Chi Y., Zheng W., Shi H., Sun J., Fu Z. Spatial heterogeneity of estuarine wetland ecosystem health influenced by complex natural and anthropogenic factors. *Science of the Total Environment*, **2018**, *634*, 1445-1462 https://doi.org/10.1016/j.scitotenv.2018.04.085
5. Fujian Water Resources and Hydropower Institute. Comprehensive Planning of Fujian Dzhangxi Basin Repot, 2014, China.
6. Gupta K, Kumar P, Pathan S.K., Sharma K.P. Urban neighborhood green index - A measure of green spaces in urban areas. *Landscape and Urban Planning*, **2012**, *105*, 325－335.
7. https://doi.org/10.1007/s11434-006-0457-1 (in Chinese)
8. https://doi.org/10.1016/j.landurbplan.2012.01.003
9. Jing Y., Zhang F., He Y., Kung H. te., Johnson V. C., Arikena M. Assessment of spatial and temporal variation of ecological environment quality in Ebinur Lake Wetland National Nature Reserve, Xinjiang, China. *Ecological Indicators*, **2020**, *110*. 105874 https://doi.org/10.1016/j.ecolind.2019.105874
10. Kurbanov E.A. Two decades of vegetation cover research with the use of MODIS. *Forest ecosystems under climate change: biological productivity and remote sensing*, **2016**, *2*, 123-132 (in Russian).
11. Kurbanov E.A., Vorobyev O.N., Gubayev A.V., Lezhnin S.A., Polevshikova Y.A., Demisheva E.N. Four decades of forest research with the use of Landsat Images. *Vestnik of Volga State University of Technology. Ser. Forest. Ecology. Nature Management*. **2014**, *21*, 18-32 (in Russian).
12. Li W., Yi P., Zhang D., Zhou Y. Assessment of coordinated development between social economy and ecological environment: Case study of resource-based cities in Northeastern China. *Sustainable Cities and Society*, **2020**, *59*. https://doi.org/10.1016/j.scs.2020.102208
13. Liu Q., Wu J., Li L., Yu L., Li J., Xin X., et al. Ecological environment monitoring for sustainable development goals in the Belt and Road region. *Journal of Remote Sensing (Chinese)*, **2018**, *22*, https://doi.org/10.11834/jrs.20187264
14. Liu R, Zhu D.L. Discussion on land use change information mining method based on transfer matrix. *Resource science*, **2010**, *32*, 1544-1550 (in Chinese).
15. Luo L. Simulation of net primary productivity (NPP) of Western Songnen grassland based on remote sensing mechanism model. Changchun: Northeast Institute of geography and agricultural ecology, Chinese Academy of Sciences, 2010. (in Chinese)
16. Meng Y., Zhao G.X. Ecological environment condition evaluation of estuarine area based on quantitative remote sensing - a case study in Kenli County. *China Environmental Science,* **2009**, *29*, 163–167. (in Chinese)
17. Miao C.L., Sun L.Y., Yang L. The studies of ecological environmental quality assessment in Anhui Province based on ecological footprint. *Ecological Indicators*, **2016**, *60, 879-883* https://doi.org/10.1016/j.ecolind.2015.08.040
18. Niu Y.Q., Wang S.L. Research on coupling relationship between fragile ecological environment and poverty in Gansu province. *Acta Ecologica Sinica*, **2017**, *37*, 6431–6439 (in Chinese).
19. Ostrom E. A general framework for analyzing sustainability of social-ecological systems. *Science*, **2009**, *325*, 419-422. https://doi.org/10.1126/science.1172133
20. State Environmental Protection Administration. Environmental protection industry standard (Trial) HJT192-2006. (in Chinese)
21. Thornthwaite C.W. An approach toward a rational classification of climate. *Geographical Review*, **1948**, 38: 55-94. DOI: 10.2307/210739
22. Vorobyev O.N., Kurbanov E.A., Gubayev A.V., Demisheva E.N. Method of stepwise classification of satellite images for the thematic mapping of forest cover. *Vestnik of Volga State University of Technology. Ser. Forest. Ecology. Nature Management*. **2015**, *28*, 57-72 (in Russian).
23. Wang C., Jiang Q., Shao Y., Sun S., Xiao L., Guo J. Ecological environment assessment based on land use simulation: A case study in the Heihe River Basin. *Science of the Total Environment*, **2019**, *697*. https://doi.org/10.1016/j.scitotenv.2019.133928
24. Wang C., Yue T., Fan Z. Solar Radiation Climatology Calculation in China. *Journal of Resources and Ecology*, **2014**, *5*, 132-138. DOI:10.5814/j.issn.1674-764x.2014.02.005
25. Wang J., Sui L., Yang X., Wang Z., Ge D., Kang J., et al. Economic globalization impacts on the ecological environment of inland developing countries: A case study of Laos from the perspective of the land use/cover change. *Sustainability* (Switzerland), **2019**, *11*, 3940 https://doi.org/10.3390/su11143940
26. Xu H.Q. A new remote sensing index for fast extraction of impervious surface. Journal of Wuhan University: *Information Science Edition*, **2008**, *33*, 1150-1153 (in Chinese)
27. Xu H.Q. Extraction of water information by improved normalized difference water index (MNDWI). *Acta remote sensing*, **2005**, *5*, 589-595 (in Chinese)
28. Xu H.Q. A remote sensing urban ecological index and its application. *Acta Ecologica Sinica*，**2013**，33, 7853-7862. (in Chinese)
29. Zhang T.Y., Wang L., Wang H., Peng L., Luo C. Remote sensing monitoring of ecological environment in salinized irrigation areas of Manas river basin. *Acta Ecologica Sinica*, **2017**, *37*, 3009–3018 (in Chinese)
30. Zhang Y., Song W., Fu S., Yang D. Decoupling of land use intensity and ecological environment in Gansu province, China. *Sustainability (Switzerland)*, **2020**, *12*, 2779 https://doi.org/10.3390/su12072779

31. Zheng J., Hu Y., Boldanov T., Bazarzhapov T., Meng D., Li Y., et al. Comprehensive assessment of the coupling coordination degree between urbanization and ecological environment in the Siberian and Far East Federal Districts, Russia from 2005 to 2017. *PeerJ-Life and Environment*, **2020**, 6. https://doi.org/10.7717/peerj.9125
32. Zhou G.S, Zhang X.S. Net primary productivity of natural vegetation in China under global climate change. *Acta phytoecology*, **1996**, *1*, 11-19 (in Chinese)
33. Zhou G.S, Zhang X.S. Preliminary study on net primary productivity model of natural vegetation. *Acta phytoecology*, **1995**, *3*, 193-200 (in Chinese)
34. Zhu J.W., Xie X.T., Xin H.L. Research on evaluation of ecological environment carrying capacity - taking HeNan province as an example. *Acta Ecologica Sinica*, **2017**, *37*, 1–9 (in Chinese)
35. Zhu W.Q., Pan Y.Z., He H, Yu D.Y., Hu H-B. Simulation of maximum light use efficiency for some typical vegetation types in China. *Chinese Science Bulletin*, **2006**, *51*, 457-463.